


## Molecular beam epitaxy growth of monolayer hexagonal $MnTe_2$ on Si(111) substrate

S Lu(卢帅), K Peng(彭坤), P D Wang(王鹏栋), A X Chen(陈爱喜), W Ren(任伟), X W Fang(方鑫伟), Y Wu(伍莹), Z Y Li(李治云), H F Li(李慧芳), F Y Cheng(程飞宇), K L Xiong(熊康林), J Y Yang(杨继勇), J Z Wang(王俊忠), S A Ding(丁孙安), Y P Jiang(蒋烨平), L Wang(王利), Q Li(李青), F S Li(李坊森), and L F Chi(迟力峰)

**Citation:**Chin. Phys. B, 2021, 30 (**12**): 126804. DOI: 10.1088/1674-1056/ac2e63
Journal homepage: http://cpb.iphy.ac.cn; http://iopscience.iop.org/cpb

**What follows is a list of articles you may be interested in**

---

## Moiré superlattice modulations in single-unit-cell FeTe films grown on $NbSe_2$ single crystals

Han-Bin Deng(邓翰宾), Yuan Li(李渊), Zili Feng(冯子力), Jian-Yu Guan(关剑宇), Xin Yu(于鑫), Xiong Huang(黄雄), Rui-Zhe Liu(刘睿哲), Chang-Jiang Zhu(朱长江), Limin Liu(刘立民), Ying-Kai Sun(孙英开), Xi-Liang Peng(彭锡亮), Shuai-Shuai Li(李帅帅), Xin Du(杜鑫), Zheng Wang(王铮), Rui Wu(武睿), Jia-Xin Yin(殷嘉鑫), You-Guo Shi(石友国), and Han-Qing Mao(毛寒青)

Chin. Phys. B, 2021, 30 (**12**): 126801. DOI: 10.1088/1674-1056/ac0816

## Epitaxial fabrication of two-dimensional $TiTe_2$ monolayer on Au(111) substrate with Te as buffer layer

Zhipeng Song(宋志朋), Bao Lei(雷宝), Yun Cao(曹云), Jing Qi(戚竞), Hao Peng(彭浩), Qin Wang(汪琴), Li Huang(黄立), Hongliang Lu(路红亮), Xiao Lin(林晓), Ye-Liang Wang(王业亮), Shixuan Du(杜世萱), Hong-Jun Gao(高鸿钧)

Chin. Phys. B, 2019, 28 (**5**): 056801. DOI: 10.1088/1674-1056/28/5/056801

## High quality $PdTe_2$ thin films grown by molecular beam epitaxy

En Li(李恩), Rui-Zi Zhang(张瑞梓), Hang Li(李航), Chen Liu(刘晨), Geng Li(李更), Jia-Ou Wang(王嘉鸥), Tian Qian(钱天), Hong Ding(丁洪), Yu-Yang Zhang(张余洋), Shi-Xuan Du(杜世萱), Xiao Lin(林晓), Hong-Jun Gao(高鸿钧)

Chin. Phys. B, 2018, 27 (**8**): 086804. DOI: 10.1088/1674-1056/27/8/086804

## Growth and transport properties of topological insulator $Bi_2Se_3$ thin film on a ferromagnetic insulating substrate

Shanna Zhu(朱珊娜), Gang Shi(史刚), Peng Zhao(赵鹏), Dechao Meng(孟德超), Genhao Liang(梁根豪), Xiaofang Zhai(翟晓芳), Yalin Lu(陆亚林), Yongqing Li(李永庆), Lan Chen(陈岚), Kehui Wu(吴克辉)

Chin. Phys. B, 2018, 27 (**7**): 076801. DOI: 10.1088/1674-1056/27/7/076801

## Two crucial factors influencing quality of GaAs on Ge substrate

Deng Chuang, Men Chuan-Ling, Chen Da

Chin. Phys. B, 2014, 23 (**4**): 046805. DOI: 10.1088/1674-1056/23/4/046805

---

RAPID COMMUNICATION

# Molecular beam epitaxy growth of monolayer hexagonal $MnTe_2$ on Si(111) substrate*

S Lu(卢帅)[1,2,†], K Peng(彭坤)[1,2,†], P D Wang(王鹏栋)[2,†], A X Chen(陈爱喜)[2], W Ren(任伟)[2,5], X W Fang(方鑫伟)[2,5], Y Wu(伍莹)[2], Z Y Li(李治云)[2], H F Li(李慧芳)[2,3], F Y Cheng(程飞宇)[2], K L Xiong(熊康林)[2], J Y Yang(杨继勇)[4], J Z Wang(王俊忠)[4], S A Ding(丁孙安)[2,5], Y P Jiang(蒋烨平)[3], L Wang(王利)[2,‡], Q Li(李青)[1,§], F S Li(李坊森)[2,5,¶], and L F Chi(迟力峰)[1]

[1] *Institute of Functional Nano & Soft Materials (FUNSOM), Soochow University, Suzhou* 215123, *China*

[2] *Vacuum Interconnected Nanotech Workstation (Nano-X), Suzhou Institute of Nano-Tech and Nano-Bionics (SINANO), Chinese Academy of Sciences (CAS), Suzhou* 215123, *China*

[3] *Key Laboratory of Polar Materials and Devices (MOE), Department of Electronic, School of Physics and Electronic Science, East China Normal University, Shanghai* 200241, *China*

[4] *School of Physical Science and Technology, Southwest University, Chongqing* 400715, *China*

[5] *School of Nano-Tech and Nano-Bionics, University of Science and Technology of China, Hefei* 230026, *China*

(Received 23 August 2021; revised manuscript received 4 October 2021; accepted manuscript online 11 October 2021)

Monolayer $MnTe_2$ stabilized as 1T structure has been theoretically predicted to be a two-dimensional (2D) ferromagnetic metal and can be tuned via strain engineering. There is no naturally van der Waals (vdW) layered $MnTe_2$ bulk, leaving mechanical exfoliation impossible to prepare monolayer $MnTe_2$. Herein, by means of molecular beam epitaxy (MBE), we successfully prepared monolayer hexagonal $MnTe_2$ on Si(111) under Te rich condition. Sharp reflection high-energy electron diffraction (RHEED) and low-energy electron diffraction (LEED) patterns suggest the monolayer is atomically flat without surface reconstruction. The valence state of $Mn^{4+}$ and the atom ratio of ([Te]:[Mn]) further confirm the $MnTe_2$ compound. Scanning tunneling spectroscopy (STS) shows the hexagonal $MnTe_2$ monolayer is a semiconductor with a large bandgap of $\sim 2.78$ eV. The valence-band maximum (VBM) locates at the $\Gamma$ point, as illustrated by angle-resolved photoemission spectroscopy (ARPES), below which three hole-type bands with parabolic dispersion can be identified. The successful synthesis of monolayer $MnTe_2$ film provides a new platform to investigate the 2D magnetism.

**Keywords:** molecular beam epitaxy, hexagonal $MnTe_2$, band structure

**PACS:** 68.37.Ef, 73.20.At, 81.15.–z **DOI:** 10.1088/1674-1056/ac2e63

## 1. Introduction

Two-dimensional (2D) materials have attracted extensive attention since the discovery of graphene.[1] When thinned to the monolayer limit, 2D materials will exhibit unique electronic and optical properties such as superconductivity[2–4] and charge density waves (CDW).[5–7] In particular, ferromagnetic and antiferromagnetic materials would be a significant addition to the family of 2D materials due to their potential application in the next-generation spintronic devices with stable storage, faster response, and low-power dissipation.[8] The recent experimental breakthrough was the observation of quantum anomalous Hall effect (QAHE) in intrinsic magnetic topological insulator $MnBi_2Te_4$,[9] in which the magnetism originates from the magnetic Mn–Te layers[10] with the high-ordered magnetism distribution in the crystal.[11] In the $MnBi_2Te_4$ system, each Mn atom is bonded with six neighboring Te atoms, which form octahedral (1T) structure $MnTe_2$. The monolayer $MnTe_2$ was predicted as a candidate for 2D ferromagnetic material.[12] To the best of our knowledge, no experimental investigation about the epitaxial growth of monolayer hexagonal $MnTe_2$ has been reported.

Manganese telluride (MnTe) has been demonstrated as a promising thermoelectric material.[13] NiAs-type MnTe (hexagonal MnTe, H-MnTe) bulk is a diluted magnetic material, exhibiting antiferromagnetic property with a Néel temperature ($T_N$) of 310 K.[14] And it is a p-type semiconductor with a small bandgap of 1.37–1.52 eV.[15] The lattice constant is $a = b = 4.158$ Å, $c = 6.726$ Å[16] and the magnetic order of H-MnTe has been determined to be in-plane ferromagnetic layers stacking antiferromagnetically along the $c$-axis.[17,18] Room temperature ferromagnetism was observed in

*Project supported by the National Natural Science Foundation of China (Grant Nos. 11604366, 11634007, 21872099, and 22072102) and the National Natural Science Foundation of Jiangsu Province, China (Grant No. BK 20160397). F. S. L. acknowledges support from the Youth Innovation Promotion Association of Chinese Academy of Sciences (Grant No. 2017370).

†Corresponding author. E-mail: These authors contributed equally to this work.

‡Corresponding author. E-mail: lwang2017@sinano.ac.cn

§Corresponding author. E-mail: liqing@suda.edu.cn

¶Corresponding author. E-mail: fsli2015@sinano.ac.cn

© 2021 Chinese Physical Society and IOP Publishing Ltd 

thick MnTe film prepared by molecular beam epitaxy (MBE) technique.[19] There is no experimental report about the two-dimensional limit of MnTe, where a Mn atom layer sandwiched between two Te layers. Recently, the DFT calculations suggest that when thinned the H-MnTe to the monolayer limit, $MnTe_2$ can stabilize as 1T-structure and is an intrinsic ferromagnetic metal.[12] There is a pyrite cubic structured three-dimensional $MnTe_2$, which was reported to be a p-type semiconductor,[20] quite different from hexagonal MnTe, focusing on its potential thermoelectric applications.[21] Therefore, the experimental realization of the monolayer $MnTe_2$ is important and promising for 2D magnetism.

Here we report an epitaxial growth of high-quality hexagonal monolayer $MnTe_2$ on Si(111)-$(7\times7)$ substrate by means of MBE. The structure and component were characterized by combining *in-situ* scanning tunneling microscopy (STM), reflection high-energy electron diffraction (RHEED), low-energy electron diffraction (LEED), angle-resolved photoemission spectroscopy (ARPES), and x-ray photoelectron spectroscopy (XPS). STM and RHEED measurements show an $MnTe_2$ monolayer with a lattice of $\sim 4.1$ Å and the height of $\sim 5$ Å on Si(111) substrates. A large bandgap of $\sim 2.78$ eV is observed with semiconducting properties in the $MnTe_2$ monolayer. Three hole-type bands with parabolic-type dispersion are observed by the ARPES measurements and the valence-band maximum (VBM) locates at $\Gamma$ point. Our work clearly shows the successful growth of a two-dimensional semiconducting $MnTe_2$ monolayer.

## 2. Experimental methods

Epitaxial growth of monolayer $MnTe_2$ on the Si(111) was carried out in a combined ultrahigh vacuum (UHV) system with a base pressure better than $3\times10^{-10}$ mbar. Prior to the film growth, the clean Si(111)-$(7\times7)$ substrates were obtained by multi-cycle flashing to $\sim 1320$ K. High purity Mn (99.98%) and Te (99.9999%) were co-evaporated from standard Knudsen cells (K-cell). The growth rate of the $MnTe_2$ film was estimated to be 0.05 ML/min, mainly determined by the flux of the Mn source. RHEED was used to monitor the crystallinity and surface morphology during the growth. The surface morphology and electronic structure were further characterized by *in-situ* STM at room temperature using a tungsten tip. The differential $\mathrm{d}I/\mathrm{d}V$ spectra were acquired by standard lock-in techniques ($f = 973$ Hz, $T = 300$ K). All the STM images were treated by using the WSxM software.[22]

By transferring via the UHV tubes (base pressure better than $2\times10^{-10}$ mbar) in Nano-X, the band structure and surface component of the monolayer $MnTe_2$ can be measured *in-situ* by ARPES and XPS, respectively. Monochromatized He-I$\alpha$ light source (21.21 eV) was used in the ARPES measurement with a VG DA30L analyzer. The energy resolution and angular resolution were better than 30 meV and 0.1°, respectively. XPS measurements were carried out by using a PHI 5000 Versaprobe II system equipped with a monochromatic Al $K\alpha$ (1486.6 eV) x-ray source. The core level and valance band structure spectra were calibrated against C–C 1s (binding energy is around 284.8 eV).

## 3. Results and discussion

Mn–Te compounds in bulk and thick films normally crystallize into NiAs-type MnTe with Mn : Te $\sim$ 1 : 1. To stabilize monolayer $MnTe_2$ with Te termination, we introduced the molecular beam epitaxy method with the help of substrate and Te-rich atmosphere. Prior to the film growth, the Si(111) substrates were first degassed at 820 K for more than 10 h, followed by multi-cycle flashing at $\sim 1320$ K for 10 s each time. The sample temperature was monitored by an infrared pyrometer. After such procedure, atomically clean Si(111)-$(7\times7)$ surfaces can be obtained, confirmed by the sharp RHEED spots in Fig. 1(a). During the film growth, the Si(111) substrate was kept at 573 K. The flux ratio of Te/Mn was about 10:1. The RHEED pattern in Fig. 1(b) shows sharp streaky lines from a thin film and bright spots from the Si(111) substrate ($a_{\mathrm{Si(111)}} \sim 3.85$ Å), demonstrating epitaxial growth with an atomically flat surface. The lattice constant of the monolayer $MnTe_2$ can be estimated to be $\sim 4.1$ Å, just slightly smaller than the lattice constant of bulk H-MnTe ($a = 4.158$ Å), quite different from the value obtained in DFT calculations.[12] The hexagonal LEED pattern in Fig. 1(c) rules out the possibility of pyrite cubic structured $MnTe_2$. No surface reconstruction was found. The fact of only one set of hexagonal LEED pattern indicates monolayer $MnTe_2$ with a single orientation, despite the high mismatch ($\sim 8\%$) between the monolayer $MnTe_2$ and the substrate. Spots of the Si(111) substrate could not be observed after the surface was completely covered with monolayer $MnTe_2$ (see Fig. S1 in the supplementary material for details).

The STM image in Fig. 1(d) shows the surface morphology of sub-monolayer $MnTe_2$ grown on Si(111). Similar to the monolayer $WTe_2$[23] and $WSe_2$,[24] distributed $MnTe_2$ islands were observed when the sub-monolayer was grown. All the islands exhibit the same height of $\sim 500$ pm, according to the line profile in Fig. 1(e). In the bulk of hexagonal MnTe, the thickness of the Mn–Te layer along $c$ direction is $\sim 1.68$ Å. Given the height of the monolayer islands, the film could be Te–Mn–Te or Mn–Te–Mn–Te. To further confirm the structure and surface compounds, *in-situ* XPS measurements were needed, as shown below. Figure 1(f) shows the typical $\mathrm{d}I/\mathrm{d}V$ spectrum of the monolayer $MnTe_2$. We can observe a big bandgap across the Fermi level. The VBM locates at $-1.20$ eV and the conduction-band minimum locates

at 1.58 eV, indicating a bandgap size of ∼ 2.78 eV. Such value is larger than the one in bulk H-MnTe (1.37 eV–1.52 eV).[15] But it is quite different from the predicted metallic property in DFT calculation.[12,32] Maybe it is due to the varied lattice constants. A small lattice constant of 3.8 Å was obtained in the DFT calculation.[12]

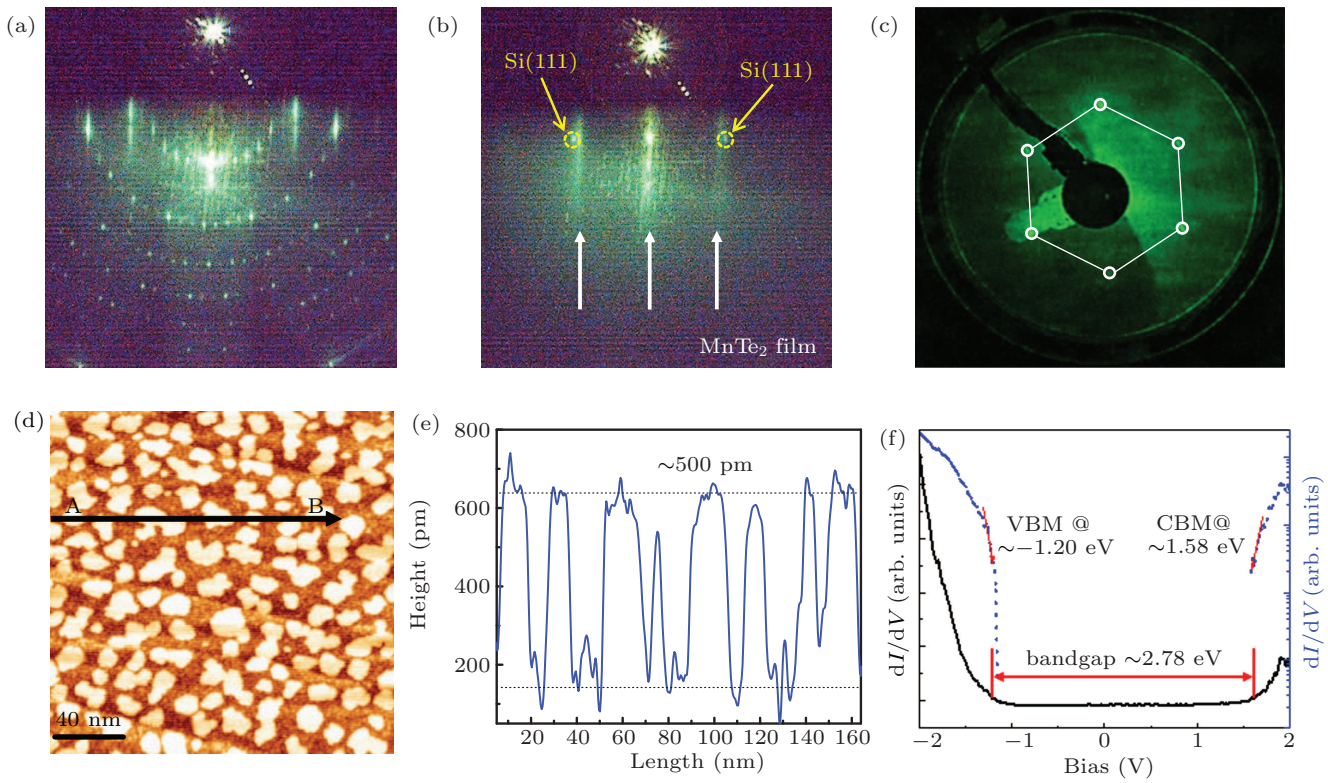



**Fig. 1.** Growth of monolayer $MnTe_2$ film on the Si(111) substrate. (a) RHEED pattern of the flashed Si(111) substrate, showing typical $(7\times7)$ reconstruction spots. (b) RHEED pattern of the sub-monolayer $MnTe_2$. White lines mark the pattern of film, while the yellow dotted circles indicate the Si(111) substrate. (c) LEED pattern image of the monolayer $MnTe_2$, clearly showing a hexagonal structure. (d) Large-scale STM image of 0.5 ML $MnTe_2$, showing the surface morphology (200 nm×200 nm). Scanning condition: $V_s = 2.0$ V, $I_t = 20$ pA. (e) Line profile of the black arrow AB in panel (d), showing all the monolayer $MnTe_2$ islands have with the same height of ∼ 500 pm. (f) Typical $dI/dV$ spectrum on the monolayer $MnTe_2$, showing the semiconducting gap size of ∼ 2.78 eV. Blue curve is the logarithmic plot.

No oxidation signal from the monolayer $MnTe_2$ can be observed in the survey XPS spectrum (see Fig. S2 in the supplementary material) after the growth and transferring process. Figures 2(a)–2(c) show the XPS spectra of Mn 3s, Mn 2p, and Te 3d core-levels, respectively. In Fig. 2(a), the Mn 3s spectra can be deconvoluted into two peaks due to the coupling of the nonionized 3s electron with 3d valence-band electrons in Mn, with the binding energies of 83.43 eV and 88.13 eV, respectively. The energy difference ($\Delta E_{3s}$) is ∼ 4.7 eV, indicating that the valence state of Mn is mainly +4 in the monolayer film.[25] Due to the complexity of Mn 2p spectrum with the splitting of 11.5 eV, we have performed a detailed deconvolution analysis in Fig. 2(b). Peak 1 of 640.6 eV corresponds to the low charge state of $Mn^{q+}$ $(0 < q < 1)$, similar to the situation in $MnBi_2Te_4$ film.[22] The low charge state of Mn was found to come from nanoclusters of manganese subtelluride induced by $Ar^+$ ion sputtering in MnTe film.[26,27] We prefer the $Mn^{q+}$ $(0 < q < 1)$ charge state may originate from the charge transfer between $MnTe_2$ film and the Si(111) substrate. Peak 2 of 641.9 eV belongs to the Mn–Te bonds of $MnTe_2$. Peaks 3 and 4 are the satellite peaks of peaks 1 and 2, respectively. The satellites in Mn 2p spectrum originate from the charge transfer between the outer electron shell of the ligand and an unfilled 3d shell of Mn during the creation of a core-hole in the photoelectron process.[28] In Fig. 2(c), the peaks at 583.9 eV and 573.5 eV are assigned to the Te $3d_{3/2}$ and $3d_{5/2}$ orbitals with a splitting of 10.4 eV, respectively.

According to the peak and the relative sensitivity factor, we can calculate the chemical composition, the atom ratio of ([Mn]:[Te]) ∼ 1 : 2.6. Judging from the valence state of +4 and atom ratio of 1:2.6, we can conclude that the grown monolayer is $MnTe_2$, as shown in Fig. 2(f). The larger Te ratio in the samples should be ascribed to the Te passivation layer between $MnTe_2$ and Si(111) substrate, which offers an atomically flat template for the film growth by saturating the dangling bonds on the Si(111) substrate.[29] The Te passivation layer may be helpful for the growth of monolayer $MnTe_2$ with a large mismatch to Si(111) substrate. Such a Te-rich-atmosphere growth method has been widely used in the growth of $Bi_2Te_3$ film on Si(111) substrate.[30] Figure S2(b) shows the cut-off edge of UPS spectra with the sample biased to −5 V. The work function (∼ 4.76 eV) of monolayer $MnTe_2$ can be calculated by using the formula $\phi = h\nu - \mathrm{SECO} - 5$, in which the secondary electron cut-off (SECO) is obtained from a linear ex-

trapolation, as shown in the inset of Fig. 2(d). The valence band maximum of ∼ 1.32 eV can also be extracted in Fig. 2(e) by linear extrapolation, which agrees well with our STS measurement in Fig. 1(f). Figure S2(c) gives the band structure of monolayer MnTe, extracted from XPS and STS measurements. Thus, we can draw the constructed band diagram of the monolayer $MnTe_2$ on Si(111). Figure 2(f) shows the top and side views of the monolayer 1T-$MnTe_2$ respectively. The octahedral 1T structure is consistent with the previous DFT calculation results.[12]

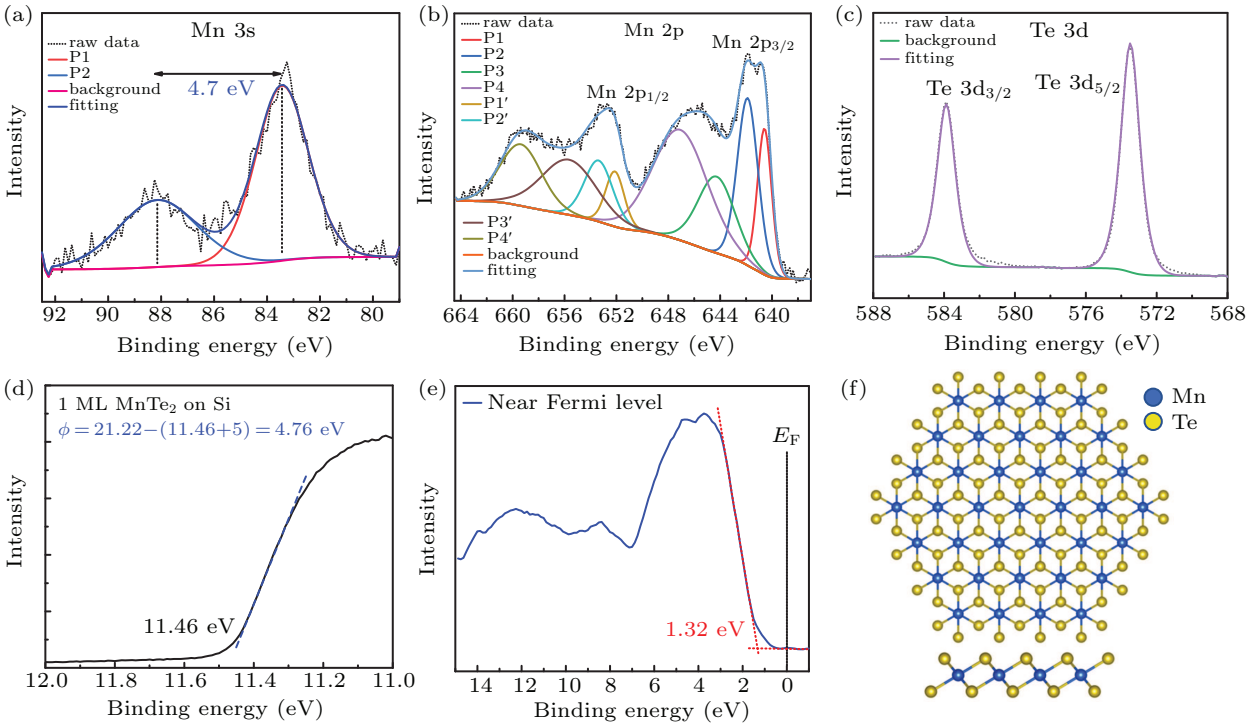



**Fig. 2.** XPS measurements of the monolayer $MnTe_2$ on Si(111). (a)–(c) The core-level spectra of Mn 3s, Mn 2p, and Te 3d. The spaced double peaks (∼ 4.7 eV) in Mn 3s suggest that the valence state of Mn is +4. The core-level spectrum of Mn $2p_{3/2}$ can be deconvoluted into four peaks. (d) UPS measurement of monolayer $MnTe_2$, showing the work function of ∼ 4.76 eV. (e) Valence-band maximum of $MnTe_2$ film. (f) Top and side view model of monolayer $MnTe_2$. The blue and yellow balls represent Mn and Te atoms, respectively.

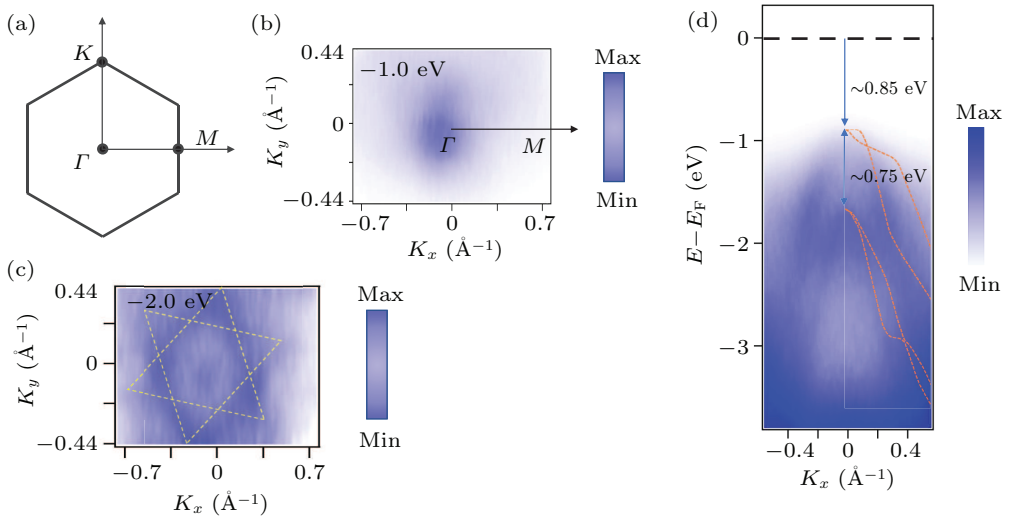



**Fig. 3.** Electronic band structure of the monolayer 1T-$MnTe_2$ on Si(111) substrate. (a) The Brillouin zone of monolayer $MnTe_2$. (b) The momentum space mapping at the energy of −1.0 eV, near the VBM. (c) The momentum space mapping at the energy of −2.0 eV. (d) The band structure measured along $\Gamma$–$M$ direction.

To further explore the electronic structure of monolayer $MnTe_2$/Si(111) heterostructures, we performed ARPES measurement at room temperature. To the best of our knowledge, ARPES observations on bulk or thin film MnTe materials have been rarely reported. Figure 3(a) shows the Brillouin zone of the hexagonal $MnTe_2$ monolayer. The momentum space mapping at −1.0 eV in Fig. 3(b) shows only hole pockets at $\Gamma$ point with VBM at ∼ −0.85 eV, consistent with the gaped structure obtained from the STS and XPS measurements. We notice that in bulk MnTe the VBM is also predicted at $\Gamma$

point theoretically.[31] The mapping at −2.0 eV in Fig. 3(c) shows a typical hexagonal structure with hole pockets. Figure 3(d) shows the band structure of monolayer $MnTe_2$ along the $\Gamma$–$M$ direction. Three hole-type bands with parabolic-type dispersion and "$M$"-shape dispersion at a deeper level are observed. Overall band shapes are similar to those of bulk MnTe[31] or 1T-$MnTe_2$ monolayer.[12,32] Here we find that the low two parabolic bands seem to overlap together. The energy difference between the upper parabolic bands and the lower ones is about 0.75 eV. The observed band structure is quite different from that of the Si(111) substrate, as shown in Fig. S3. Clean Si(111)-$(7 \times 7)$ substrate shows nearly linear dispersion along the $\Gamma$–$M$ direction. The surface states of S1, S2, and S3 can be identified at 0.20 eV, 0.90 eV, and 1.8 eV below the Fermi level, respectively.[33] After the growth of monolayer $MnTe_2$, no surface state and other band structures from Si(111) surface can be observed. According to previous DFT calculations,[12,32] monolayer $MnTe_2$ was predicted to be metallic. Our observations suggest monolayer hexagonal $MnTe_2$ exhibits semiconducting properties with considerable bandgap ($\sim$ 2.78 eV) at room temperature, larger than that of bulk MnTe (1.37 eV–1.52 eV).[15] One possibility is the varied lattice constant. As predicted,[32] the lattice strain can open a bandgap in $MnTe_2$ monolayer. However, the predicted bandgap is much smaller than the one in our experiment, which deserves further detailed calculations.

We would like to discuss more about the formation of hexagonal $MnTe_2$ monolayer. In previous MBE growth, thick MnTe film crystallized into NiAs-type phase on the Si(111)[19] and InP(111),[34] while the preparation of a monolayer thin film failed. As shown in Fig. S4, if further increasing the coverage, several islands with the height of $\sim$ 330 pm were observed on the monolayer $MnTe_2$, beside the second $MnTe_2$ layer with the height of $\sim$ 670 pm. It demonstrates the competition between the formation of bulk MnTe and van der Waals layered $MnTe_2$. The interaction with the substrate can stabilize the monolayer $MnTe_2$. The successful grown monolayer $MnTe_2$ is an important step to investigate the intrinsic 2D ferromagnetic properties due to its in-plane ferromagnetic order with single-layer Mn atoms.

## 4. Conclusion

In summary, we have successfully synthesized the hexagonal monolayer $MnTe_2$ film on Si(111) substrate by means of MBE. By combing *in-situ* STM, LEED, XPS, and ARPES, we have demonstrated atomically flat hexagonal monolayer $MnTe_2$ film with a large bandgap of $\sim$ 2.78 eV. The core-level spectrum of Mn 3s suggests the valence state of Mn is mainly +4. The atomic ratio of ([Te]:[Mn]) $\sim 2.6:1$ not only verifies the component of $MnTe_2$, but also implies the existence of Te passivation layer on Si(111) surface, which facilitates the epitaxial growth of $MnTe_2$ with large lattice mismatch. ARPES results show that the VBM is at $\Gamma$ point with an energy of −0.85 eV. Clear three bands with parabolic-type dispersion can be observed, agreeing well with the band shapes of bulk MnTe[31] or 1T-$MnTe_2$ monolayer. Our work offers an opportunity to investigate the electronic and magnetism properties of MnTe materials with thickness down to two-dimensional limit as $MnTe_2$.

## References


[1] Novoselov K S, Geim A K, Morozov S V, Jiang D, Zhang Y, Dubonos S V, Grigorieva I V and Firsov A A 2004 *Science* **306** 666
[2] Zhang T, Cheng P, Li W J, Sun Y J, Wang G, Zhu X G, He K, Wang L L, Ma X C, Chen X, Wang Y Y, Liu Y, Lin H Q, Jia J F and Xue Q K 2010 *Nat. Phys.* **6** 104
[3] Wang Q Y, Li Z, Zhang W H, Zhang Z C, Zhang J S, Li W, Ding H, Ou Y B, Deng P, Chang K, Wen J, Song C L, He K, Jia J F, Ji S H, Wang Y Y, Wang L L, Chen X, Ma X C and Xue Q K 2012 *Chin. Phys. Lett.* **29** 037402
[4] Wang H, Huang X W, Lin J H, Cui J, Chen Y, Zhu C, Liu F C, Zeng Q S, Zhou J D, Yu P, Wang X W, He H Y, Tsang S H, Gao W B, Suenaga K, Ma F C, Yang C L, Lu L, Yu T, Teo E H T, Liu G T and Liu Z 2017 *Nat. Commun.* **8** 394
[5] Ugeda M M, Bradley A J, Zhang Y, Onishi S, Chen Y, Ruan W, Ojeda-Aristizabal C, Ryu H, Edmonds M T, Tsai H Z, Riss A, Mo S K, Lee D H, Zettl A, Hussain Z, Shen Z X and Crommie M F 2016 *Nat. Phys.* **12** 92
[6] Ryu H, Chen Y, Kim H, Tsai H Z, Tang S J, Jiang J, Liou F, Kahn S, Jia C H, Omrani A A, Shim J H, Hussain Z, Shen Z X, Kim K, Min B I, Hwang C, Crommie M F and Mo S K 2018 *Nano Lett.* **18** 689
[7] Zhang D M, Ha J, Baek H, Chan Y H, Natterer F D, Myers A F, Schumacher J D, Cullen W G, Davydov A V, Kuk Y, Chou M Y, Zhitenev N B and Stroscio J A 2017 *Phys. Rev. Mater.* **1** 024005
[8] Zelezny J, Wadley P, Olejnik K, Hoffmann A and Ohno H 2018 *Nat. Phys.* **14** 220
[9] Deng Y J, Yu Y J, Shi M Z, Guo Z X, Xu Z H, Wang J, Chen X H and Zhang Y B 2020 *Science* **367** 895
[10] Li J H, Li Y, Du S Q, Wang Z, Gu B L, Zhang S C, He K, Duan W H and Xu Y 2019 *Sci. Adv.* **5** eaaw5685
[11] Mong R S K and Moore J E 2019 *Nature* **576** 390
[12] Chen W, Zhang J M, Nie Y Z, Xia Q L and Guo G H 2020 *J. Magn. Magn. Mater.* **508** 166878
[13] Xu Y D, Li W, Wang C, Li J, Chen Z W, Lin S Q, Chen Y and Pei Y Z 2017 *J. Mater. Chem. A* **5** 19143
[14] Walther K 1967 *Solid State Commun.* **5** 399
[15] Mori S, Sutou Y, Ando D and Koike J 2018 *Mater. Trans.* **59** 1506
[16] Kriegner D, Vyborny K, Olejnik K, Reichlova H, Novak V, Marti X, Gazquez J, Saidl V, Nemec P, Volobuev V V, Springholz G, Holy V and Jungwirth T 2016 *Nat. Commun.* **7** 11623
[17] Mu S, Hermann R P, Gorsse S, Zhao H Z, Manley M E, Fishman R S and Lindsay L 2019 *Phys. Rev. Mater.* **3** 025403
[18] Szuszkiewicz W, Dynowska E, Witkowska B and Hennion B 2006 *Phys. Rev. B* **73** 104403
[19] Kim W, Park I J, Kim H J, Lee W, Kim S J and Kim C S 2009 *IEEE Trans. Magn.* **45** 2424
[20] Hastings J M, Elliott N and Corliss L. M 1959 *Phys. Rev.* **115** 13
[21] Xu Y D, Li W, Wang C, Chen Z W, Wu Y X, Zhang X Y, Li J Q, Lin S, Chen Y and Pei Y Z 2018 *J. Materiomics* **4** 215
[22] Horcas I, Fernandez R, Gomez-Rodriguez J M, Colchero J, Gomez-Herrero J and Baro A M 2007 *Rev. Sci. Instrum.* **78** 013705
[23] Li H F, Chen A X, Wang L, Ren W, Lu S, Yang B J, Jiang Y P and Li F S 2020 *Appl. Phys. Lett.* **117** 161601
[24] Chen W, Hu M L, Zong J Y, Xie X D, Meng Q H, Yu F, Wang L, Ren W, Chen A X, Liu G, Xi X X, Li F S, Sun J, Liu J W and Zhang Y 2021 *Adv. Mater.* **33** 2004930
[25] Biesinger M C, Payne B P, Grosvenor A P, Lau L W M, Gerson A R and Smart R S 2011 *Appl. Surf. Sci.* **257** 2717
[26] Iwanowski R J, Heinonen M H and Witkowska B 2010 *J. Alloys Compd.* **491** 13

[27] Jiao F, Wang J, Wang X, Tian Q, Chang M, Cai L, Zhu S, Zhang D, Lu Q, Wang C, Tan S, Li Y, Jing Q, Liu B and Qian D 2021 *J. Supercond. Nov. Magn.* **34** 1485

[28] Li H, Liu S S, Liu C, Zhang J S, Xu Y, Yu R, Wu Y, Zhang Y G and Fan S S 2020 *Phys. Chem. Chem. Phys.* **22** 556

[29] Lupke F, Dolezal J, Cherepanov V, Ostadal I, Tautz F S and Voigtlander B 2019 *Surf. Sci.* **681** 130

[30] Liu H W, Yuan H T, Fukui N, Zhang L, Jia J F, Iwasa Y, Chen M W, Hashizume T, Sakurai T and Xue Q K 2010 *Cryst. Growth Des.* **10** 4491

[31] Yin G, Yu J X, Liu Y Z, Lake R K, Zang J D and Wang K L 2019 *Phys. Rev. Lett.* **122** 106602

[32] Chen W, Zhang J M, Nie Y Z, Xia Q L and Guo G H 2020 *J. Phys. Chem. Solids* **143** 109489

[33] Sheverdyaeva P M, Mahatha S K, Ronci F, Colonna S, Moras P, Satta M and Flammini R 2017 *J. Phys. Condes. Matter* **29** 215001

[34] Zhang J Y, Lian Q, Pan Z Q, Bai W, Yang J, Zhang Y Y, Tang X D and Chu J H 2020 *J. Raman Spectrosc.* **51** 1383